
Novel Sensor Geolocation Technology for Detection and Discrimination of Unexploded Ordnance¹

Dorota A. Grejner-Brzezinska¹, Charles Toth^{1,2}, Hongxing Sun¹ and Xiankun Wang¹
Satellite Positioning and Inertial Navigation (SPIN) Laboratory¹
Center for Mapping²
The Ohio State University

470 Hitchcock Hall, Neil Av., Columbus OH, 43221
dbrzezinska@osu.edu
Tel. 614-292-8787, Fax: 614-292-2957

Chris Rizos
School of Surveying & Spatial Information Systems
The University of New South Wales, Sydney, Australia

c.rizos@unsw.edu.au
Tel: +61-2-93854205, Fax: +61-2-93137493

¹ Some parts of this manuscript were included in the publication by the same authors in the ION/IEEE PLANS Proceedings, May 2008 and ION GNSS Proceedings, September 2008.

ABSTRACT

Reliable and accurate geolocation is essential for robust detection, discrimination and remediation of unexploded ordnance (UXO) and other munitions and explosives-of-concern (MEC). The MEC characterization and remediation activities using the currently available detection and geolocation technologies often yield unsatisfactory results, and are extremely expensive, due mainly to the inability of the current technology to detect all MEC present at a site, and their failure to discriminate between MEC and non-hazardous items. This is a consequence of insufficiently accurate relative geolocation information of the electromagnetic (EM) sensors, since multiple EM images are combined together to produce 3D images of the buried objects, which are often blurred due to the poor sensor geolocation. As a result, most of the cost (90%) of MEC remediation involves excavating targets that pose no threat. Thus, the goal of the research presented here is to design and implement a high-accuracy device that can address the stringent navigation/geolocation requirements of a man-portable EM system in open and impeded environments, and therefore lower the cost of remediation by improving the geolocation accuracy of MEC that will result in better discrimination, by practically eliminating excavation of non-hazardous objects.

The proposed system design is based on the tight ‘quadruple’ integration of the Global Positioning System (GPS), inertial measurement unit system (IMU), terrestrial RF system – pseudolite (PL), and terrestrial laser scanning (TLS) to support high-accuracy navigation for a non-contact mapping system in GPS-challenged environments. The key novel component of the proposed multi-sensor system is the integration of TLS that can provide very high positioning accuracy in a local frame, and thus can support a GPS/INS/PL-based navigation system in achieving both absolute and relative high positioning accuracy in impeded environments.

This paper presents the concept design of the quadruple integration system, the algorithmic approach to sensor integration with a special emphasis on TLS integration with GPS/IMU/PL, and the performance assessment based on simulations and real data, where cm-level relative geolocation accuracy is demonstrated.

1 INTRODUCTION

Many formerly used defense sites, such as munitions burning and open detonation areas, and burial pits, thousands of acres in size, are still contaminated with unexploded ordnance (UXO). The detection and remediation of munitions and explosives-of-concern (MEC) on ranges, munitions burning and open detonation areas, and burial pits is one of the Department of Defense’s (DoD) most pressing environmental problems. Assessment tools that can efficiently survey large tracts of land are required, and traditional ground-based survey procedures are often too inefficient and costly. There are existing systems, such as, for example, the Multi-sensor Towed Array Detection System (MTADS) for large-scale UXO geophysical surveys (<http://www.cpeo.org/techtree/ttdescript/advnmstad.htm>). In general, depending on the type and extent of the terrain, the types and amounts of buried metal objects, airborne or land-based detection technologies must be applied. The focus here is on a land-based man-portable UXO detection system.

Geophysical mapping is the standard initial approach to investigating MEC sites and identifying potential MEC objects. In the standard practice, the first phase of geophysics work is “mag and flag,” done with the objective of screening the entire site,

and identifying some portions for further investigation (local interrogation). “Mag and flag” refers to the traditional way of finding UXO, where technicians walk survey lanes (transects) laid out in a field (see Figure 1), swinging a metal detector in front of them.

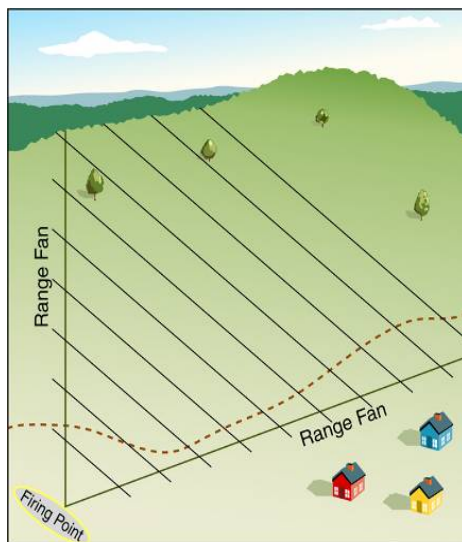


Figure 1. Defining boundaries of the target area and geophysical transect spacing based on historical data, such as, for example, Archive Search Report conducted by the Army Corps of Engineers as part of the historical records review process (http://www.epa.gov/fedfac/documents/brief_dod_091205.ppt)

The most commonly used detector for UXO is a magnetometer, hence the “mag”. However, this normally can result in thousands of points being flagged as potential MEC targets, thus, another phase of local interrogation will determine the type of buried object before the removal by excavation can be carried out. Since excavation is the most expensive part of the MEC remediation process, it is naturally desirable to limit the excavation to only those objects that pose a threat to the public and the environment (compare an example illustrated in Figure 2, which shows the difference between the anomalies detected and identified as UXO). The second phase normally involves an electromagnetic (EM) survey of the site, to provide improved geophysical data, usually along transects with increased density, over the suspected target area. It is crucial that the images acquired by the EM survey provide sufficient information to detect all MEC present at a site and to discriminate between MEC and non-hazardous items, as well to identify the type of MEC/UXO.

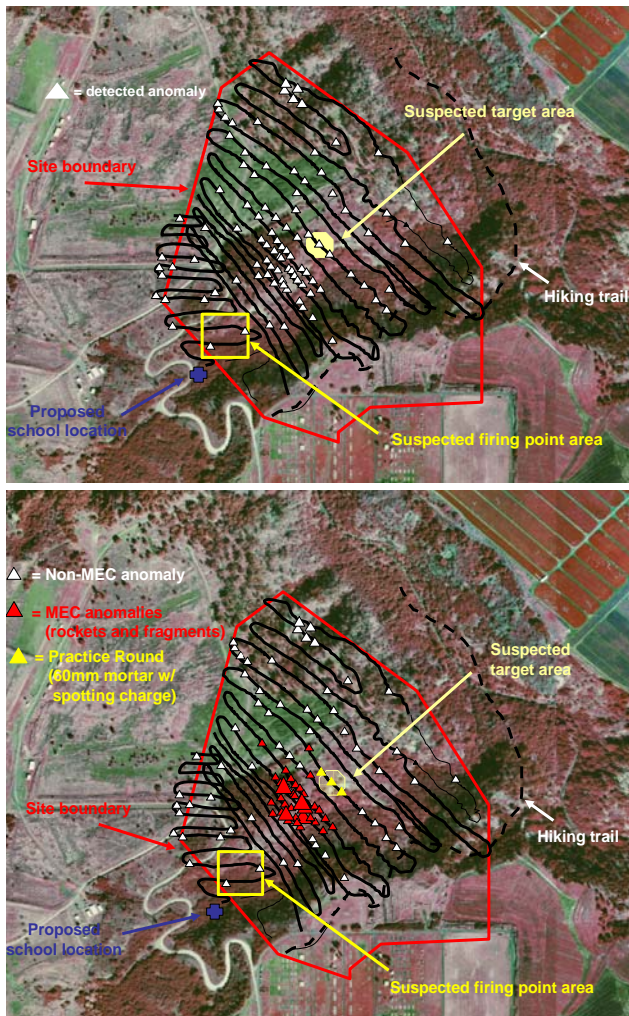


Figure 2. Detected anomalies after “mag and flag” step (top) and anomalies identified after refined geophysical mapping (bottom) (http://www.epa.gov/fedfac/documents/brief_dod_091205.ppt).

As reported by SERDP2 (2005), based on actual field experience, over 90 per cent of objects excavated during MEC site remediation are found to be non-hazardous items. In order to address this problem, the Strategic Environmental Research and Development Program (SERDP) of DoD coordinates numerous efforts aimed at developing new and improved technologies to discriminate MEC from non-hazardous subsurface items. According to SERDP, “using current sensor technologies, the best hope for such discrimination lies in detailed spatial mapping of magnetic or electromagnetic signatures. Such investigation requires geolocation technologies that function at two levels. First, anomalous signals must be coarsely located so that they can be reacquired with a required absolute accuracy of tens of centimetres. Second, detailed mapping of signatures involves the measurement of the locations of individual sensor readings to a relative accuracy on the order of

² SERDP is the DoD’s environmental science and technology program, planned and executed in full partnership with the Department of Energy and the Environmental Protection Agency, with participation by numerous other federal and non-federal organizations. To address the highest priority issues confronting the Army, Navy, Air Force, and Marines, SERDP focuses on cross-service requirements and pursues high-risk/high-payoff solutions to the Department’s most intractable environmental problems. The development and application of innovative environmental technologies support the long-term sustainability of DoD’s training and testing ranges as well as significantly reduce current and future environmental liabilities (<http://www.serdp.org/>)

roughly 1 cm. By virtue of topography or vegetation, many sites are not amenable to Differential Global Positioning System (DGPS)” (SERDP, 2005).

No navigation system currently available can meet the stringent navigation/geolocation requirements as stated above. One possible solution, as presented in this paper, is to design a hybrid system, based on various navigation and imaging technologies that offer either good absolute navigation accuracy or can support reliable relative navigation in a local frame. The level of integration and the capability of adapting the sensor and software configuration to become applicable to specific deployment scenarios are the key factors of this approach.

The range of navigation techniques applicable to this task includes satellite and terrestrial RF ranging systems, inertial navigation systems (INS), or inertial measurement units (IMU), laser scanning systems, and even electro-optical devices, such as total stations. Each individual method comes with its own limitations, which are expected to be balanced within the integrated system design, where complementary and often redundant characteristics of these sensor technologies become advantageous. The advantages and disadvantages of the sensors and their complementary characteristics are listed in Table 1. Thus, the goal of the research described in this paper is to design, implement and test a high-accuracy hybrid device that can address the stringent navigation/geolocation requirements of a man-portable geophysical mapping system, and is capable of maintaining high relative positioning accuracy in GPS-challenged environments.

The remainder of the paper is structured as follows: first, the design concept and implementation of the system are presented; then, the relative positioning model of the terrestrial laser scanning (TLS) is introduced; next, the tight GPS/PL/IMU/TLS integration is discussed; and finally, the performance assessment based on real and simulated data is presented, followed by the summary and conclusions.

2. SYSTEM DESIGN AND ARCHITECTURE

The system’s operational concept design, as illustrated in Figure 3, is based on quadruple integration of GPS, inertial technology, terrestrial RF system – pseudolite (PL), and TLS that collectively can support high-accuracy geolocation of geophysical sensors in a range of environments. The proposed design integrates PL and GPS range measurements together with the INS and TLS measurements to deliver an optimal hybrid positioning solution in a tight integration mode using the Extended Kalman Filter (EKF) algorithms. Multi-sensor integration is mandatory to assure accuracy, continuity and integrity of the navigation solution. To facilitate high relative positioning accuracy in a local frame, in GPS-challenged environments, a novel integration approach is proposed that incorporates TLS technology. To achieve an environment-invariant performance of the TLS-based positioning subsystem, easily deployable spherical ground targets are used.

The proposed three-tier positioning concept is hierarchical, with the following primary capabilities:

1. ***Absolute positioning*** in a global reference system (WGS-84), applicable to open-sky areas, achieved primarily using Differential GPS (DGPS)/IMU integration.

2. **Relative medium-range positioning** under canopies or other obstructions. The connection to WGS-84 is achieved via PL/IMU integration, where PL substitutes for the obstructed GPS signals for medium to long transmitter/receiver distances.
3. **Relative short-range positioning** in a local frame. This mode supports the detailed mapping of geophysical signatures, where both GPS and PL are not available, and where very high relative positioning accuracy is required. It is facilitated by TLS with ground-based deployable targets. Since the laser scanner reference frame is connected to the GPS/IMU/PL reference system via lever arm and boresight angles, estimated by the system calibration process, the absolute positioning in WGS84 is maintained. The accuracy of the absolute coordinates may vary as a function of the quality of the last good GPS or PL-based solution, while the relative positioning accuracy in the local frame is maintained at cm-level.

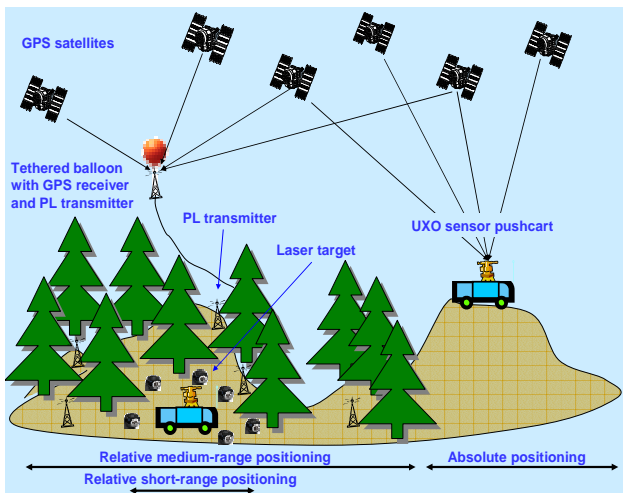


Figure 3. Three-tier MEC site survey concept.

3. NAVIGATION AND IMAGING TECHNOLOGIES

The commercial and research applications of the integrated GPS/IMU systems for imaging sensor geolocation has been steadily growing, and extensive literature on this subject exists (e.g., Abdullah, 1997; El-Sheimy and Schwarz, 1999; Grejner-Brzezinska and Toth, 1998; Grejner-Brzezinska, 1999; Grejner-Brzezinska, 2001a and b; Grejner-Brzezinska et al., 2005; Mostafa et al., 2000; Skaloud, 2002; Toth, 2002; Toth and Grejner-Brzezinska, 1998; Yi et al., 2005). However, the navigation solution accuracy provided by GPS/INS strongly depends on the quality and geometry of GPS observations, as well as the type of inertial system used and the integration model applied. Generally, under no or limited GPS availability, the navigation accuracy that satisfies the requirements of sensor geolocation can be only maintained for a few minutes if a navigation-grade IMU is used. Longer GPS gaps lead to a loss of reliable geolocation information. Thus, alternative sensors, such as PLs (e.g., LeMaster and Rock, 1999; Dai et al., 2001; Grejner-Brzezinska and Yi, 2003; Barnes et al., 2003a, b, 2005 and 2006), or imaging, optical or laser-based, systems (e.g., Veth and Raquet, 2006) must be deployed to assure accuracy and continuity of the navigation solution.

3.1. Pseudolite technology

Pseudolites are ground-based radio navigation devices, which are designed to support positioning and navigation in situations where the GNSS (Global Satellite Navigation System) constellation may be insufficient or unavailable (e.g., indoor, urban or confined environments). PLs can be configured either to emit GPS-like signals for enhancing the GPS by providing increased accuracy, integrity, and availability, or to serve as an independent navigation system transmitting on non-GPS frequencies. In addition to the increased redundancy due to the use of PL signal, the primary advantage of combining them with GPS is to improve the vertical dilution of precision (VDOP) factor.

The primary characteristics of the currently available PL technology can be summarized as follows:

- Line-of-sight (subject to signal blockage)
- Used as augmentation to GPS or as an autonomous constellation
 - GPS frequency or non-GPS frequency
- Typical signal range 3-5 km
- mm to cm-level ranging accuracy achievable
- cm to dm-level positioning accuracy in static or kinematic modes
- Single-frequency and dual-frequency systems available
- Self-contained time-synchronized constellations (such as Locata system used here) or asynchronous PL networks.

The example commercial systems currently available on the market are Terralite XPS technology from Novariant Inc. (http://www.novariant.com/resources/technologies/positioning_infrastructure.cfm) and LocataNet system from Locata Inc. (<http://www.locatacorp.com/aboutUs.html>; Barnes et al., 2003a and b).

The PL technology used in this research is LocataNet (e.g., Barnes et al., 2003a and b, and 2005), a network of dual-frequency ground-based transmitters (LocataLites) designed to cover a survey area with ranging signals of continuous coverage. These ranging signals transmit in the license-free 2.4GHz Industry Scientific and Medical (ISM) band. The LocataLite hardware design uses state of the art field programmable gate array (FPGA) devices. They provide configurable logic, on-chip memory and digital signal processing (DSP) capabilities. For signal spatial diversity, one LocataLite can be connected to two transmit antennas allowing for transmitting two signals with different PRN codes at the same frequency.

A Locata receiver uses four or more ranging signals to different LocataLites to compute a high-accuracy position entirely independent of GPS. An important feature of the Locata positioning signals is that they are time-synchronized, which allows single-point positioning similar to pseudorange-based GPS. However, unlike GPS, the sub-cm level of synchronization between LocataLites allows single-point positioning with GPS-RTK (real time kinematic) level of accuracy without the use of a reference station and data link. In addition, Locata signal strength of up to 1 Watt is significantly higher than the GPS signals, and thus offers better foliage penetration within the range of a few to tens of kilometers. It should be noted that in stand-alone mode, Locata may suffer from poor height accuracy if there is little variation in elevation angle between the terrestrial transmitters and receivers. It should be mentioned that in operational environments, the coordinates of the

LocataLite antennas are normally surveyed using GPS and total station equipment to provide WGS-84 Earth Centered Earth Fixed (ECEF) coordinates.

The high chipping rate (10MHz) results in less multipath error, because the delay in a reflected signal will rarely be more than two chips. In addition, the spatial diversity technology using two RX antennas is employed to attenuate multipath error. The spatial diversity is one the three types of signal diversity principles that are common practices in terrestrial RF communications to reduce signal fading. In spatial diversity, the receiver antenna uses multiple elements physically separated in space to improve the signal detection and receiving. With the spatial diversity technology, Locata kinematic positioning in moderately obstructed environments can provide centimeter-level quality with 100% coverage, as well as consistent geometry and high reliability (Barnes et al., 2006). Table 2 lists the primary characteristics of the LocataNet system.

3.2. Terrestrial laser scanning (TLS)

The ability of terrestrial laser scanner technology to capture large amounts of spatial data quickly, accurately and automatically makes it an important tool for spatial data and surface acquisition, even for complex surfaces and environments often inaccessible by classical survey techniques. TLS consists of an instrument for measuring distance (laser) and a scanner. The laser beam is focused, and is directly reflected of the surveyed surface, making it unnecessary to use prism reflectors. Generally, 3D environments are captured faster with TLS, as compared to alternative techniques, with the accuracy ranging from sub-millimeter on small object scans to 25 mm on objects at distances up to 250 m and spatial sampling of 0.01° (<http://www.ceg.ncl.ac.uk/heritage3d/downloads/TSA-Laser-Scan.pdf>). The output from a TLS system is a 3D point cloud (X, Y, Z coordinates in a local TLS frame that can be converted to a selected mapping frame, in which TLS location coordinates are defined). Additional details on LiDAR systems, including terrestrial laser scanning systems can be found in (Shan and Toth, 2008).

TLS in the mapping mode is normally placed at a site with known coordinates, or GPS/IMU can be used for direct geolocation if the system is located on a moving platform. However, an inverse problem can be defined, that is, if the TLS's location is unknown, it can be triangulated from the scanned objects with known locations, or, if the absolute coordinates of the scanned objects are not identified, the objects' coordinates defined in some local frame (or TLS frame) can be used to determine a change in the TLS location coordinates. This is possible by matching the multi-site scans that allows for the determination of the coordinate transformation parameters between the sites. For example, a 6-parameter similarity transformation can be established between two point clouds of the same scene (here, spherical targets were selected for their rotation invariant property) collected at locations T_1 and T_2 , as shown in Figure 4. These transformation parameters describe the change in TLS location and orientation between T_1 and T_2 that can facilitate measurement update in the integrated EKF. Thus, TLS, which is collocated with the EM sensor via known (calibrated) boresight parameters, can be used as a navigation/geolocation device for the EM sensor. This application mode of TLS is utilized in the hybrid navigation system discussed here. An added benefit of using laser is that it is an active sensor, and therefore, it displays no dependency on ambient lighting conditions that may vary significantly in vegetated areas.

In order to find the transformation parameters between the two subsequent locations of the TLS/EM system, the following steps must be accomplished, as illustrated in Figure 5: (1) scanning of the scene at T_1 , (2) determination of the spherical target coordinates in the local TLS frame at T_1 , (3) scanning of the scene at T_2 , (4) determination of the spherical target coordinates in the local TLS frame at T_2 , (5) solution of the TLS-based resection problem that is equivalent to finding the transformation parameters between locations T_1 and T_2 based on the spherical target matching observed at T_1 and T_2 .

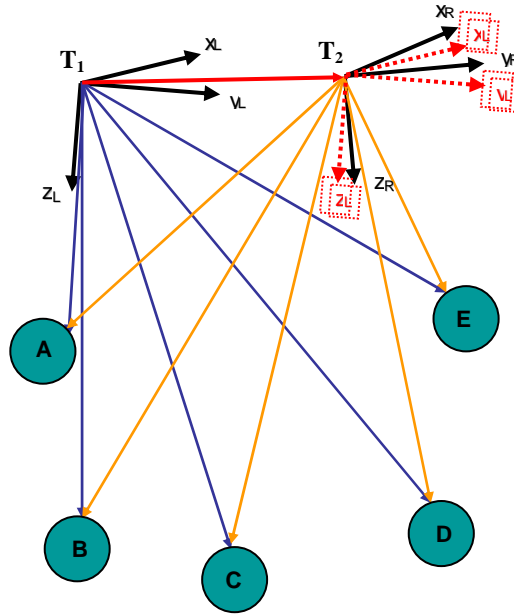


Figure 4. TLS-based navigation concept based on spherical target matching at two locations of the TLS/EM, T_1 and T_2 . Targets are denoted as A-E, the TLS coordinate system is centered at TLS and changes its location and orientation between the consecutive locations of TLS; $X_L Y_L Z_L$ and $X_R Y_R Z_R$ represent two consecutive locations/orientations of the TLS coordinate system.

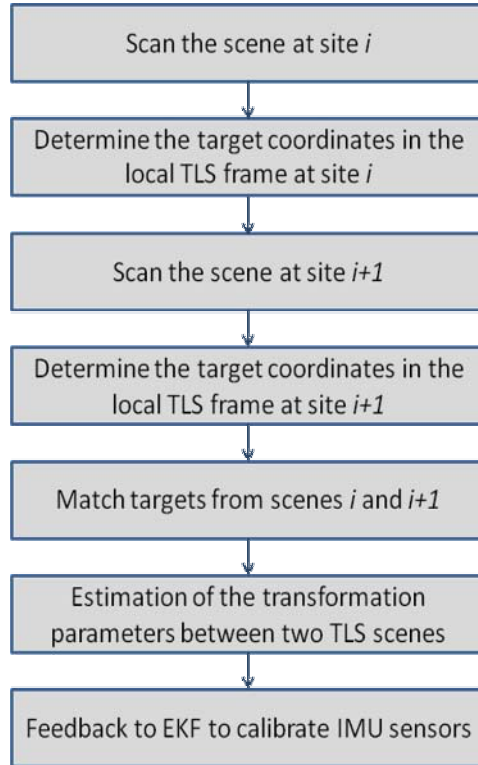


Figure 5. Flowchart of the TLS resection and transformation parameter estimation between sites i and j that are used for IMU error calibration in EKF: i and $i+1$ represent two consecutive locations of the TLS.

3.2.1. Determination of the spherical target coordinates

Determination of the spherical target center coordinates from the TLS point cloud involves the following steps.

- 1) **Look up table (LUT) indexing:** indexing TLS point cloud with a Look-up Table (LUT) is an efficient method for TLS data processing, where a link between the laser points and a two-dimensional array of azimuths and vertical angles of the points is established. LUT arranges the randomly distributed data by indexing points in space with the neighboring cells in the table, which greatly simplifies the sphere point classification algorithm. This step is optional, and applies only to data sets with unstructured point cloud.
- 2) **Sphere point classification:** two algorithms have been developed for sphere point classification: (1) shortest-range algorithm, and (2) region-growing algorithm. The shortest-range algorithm is based on finding the shortest range (distance) from the scanner to the surface of the spherical target within a search window, and selecting points with ranges within the threshold defining the shortest range ($\Delta s \leq \sqrt{s^2 - 2rs} - s$, where s is the range and r is the known radius of the spherical target). The width of the search window is set based on the scanning angle increment, expressed as the number of points scanned within the increment (e.g., 15 in the tests presented here). Next, a least squares fitting algorithm is applied to determine the approximate center candidate from the selected points on the sphere, as explained in the next section. The region-growing algorithm is based on segmentation of the points within the search window into different groups (objects), and subsequently, performing the fitting of the points from each group onto the sphere. Based on the

simulations performed to date, the region-growing algorithm was found to perform better, particularly in cases of occlusions and noisy data. See Grejner-Brzezinska et al. (2008) for the results of using the shortest-range algorithm for spherical target center determination.

Both sphere point classification algorithms are followed by the sphere center refinement procedure to assure inclusion of the maximum amount of genuine sphere points into the sphere center estimation process. Since there is a certain overlap between the search windows, two neighboring windows which cover the same sphere region will generate two approximate sphere centers. During the refinement step, the distances between the sphere center candidates are checked against the predefined threshold (0.05m in the tests presented here), and if the condition is met, the coordinates from these candidate solutions are averaged. After the shortest range, s , is calculated by means of the averaged sphere center coordinates, the search window width, D , can be determined as $D = \frac{2r\sqrt{s^2 + 2rs}}{s + r}$, to search the entire range of sphere points, and thus, to assure that a maximum number of sphere points are properly discriminated.

- 3) **Least squares fitting**: assuming that the approximate sphere center coordinates are (x_0, y_0, z_0) , the i^{th} measured sphere point is (x_i, y_i, z_i) , r is the sphere radius (known and constant), then:

$$(x_0 - x_i)^2 + (y_0 - y_i)^2 + (z_0 - z_i)^2 = r^2 \quad (1)$$

After the linearization of equation (1), the residual of the i^{th} “observed” radius can be denoted as:

$$V_i = \frac{(x_0 - x_i)}{r_i} \delta x + \frac{(y_0 - y_i)}{r_i} \delta y + \frac{(z_0 - z_i)}{r_i} \delta z + r - r_i \quad (2)$$

where $(\delta x, \delta y, \delta z)$ denote the coordinate corrections to the approximated sphere center coordinates, and r_i denotes the radius to the approximate sphere center. By employing the least squares adjustment, the corrections to the approximate sphere center coordinates can be computed by an iterative process.

- 4) **Matching of spherical targets observed from two locations of TLS**: The objective of spherical target matching is to determine the corresponding spherical target centers derived from different scans. Since it is intended to use a limited number of spherical targets in the field, the correspondence between sphere centers can be determined through a simple method that exploits the topology of the centers’ distribution.

Primarily due to occlusions, the geometric configurations of the extracted sphere centers, measured at different scanning sites vary, yet a sufficient number of line segments between the target centers are identical at both scenes. Based on this concept, the spherical target matching starts by clockwise (or anticlockwise) indexing of the sphere center points and is based on the comparison of the lengths between consecutive point pairs in the two data sets to find the matching line segment pairs. Next, the sphere center pairs between other two data sets are determined based on the condition of having the same sum of distances to the end points of the already matched line segments. Finally, the remaining end points of the line segments can be matched with the same method, that is, if an end point has the same sum of distances to the already matched points in one data set as another end point in the second data set, they are assumed to belong to the same

spherical object. Nevertheless, the distances between two identical sphere centers measured at two different scan sites differ by the accuracy of the sphere center determination, and thus, an appropriate threshold is used for the distance matching.

After the spherical target matching is complete, the coordinates of the sphere centers in the second or any subsequent data set, or local frame, can be transformed to the first local frame with a similarity transformation. Since the coordinates of the laser scanner can be coarsely determined by the INS, the transformation angles between the two data sets are usually small, and therefore, a six-parameter similarity transformation is adequate. Finally, the position and orientation changes of the system platform can be derived based on the spatial resection.

3.2.2. TLS-based resection

In the actual application, if a geophysical signal is detected during the traversing of an MEC site, the high-resolution/accuracy local survey is typically needed for cued interrogation. In this case 6-10 spherical targets are placed around the border of the area of interest (~ 10 -20 m by 10-20 m). Ideally, a near uniform distribution of the targets is desirable, but for operational purposes, depending on the terrain and the surrounding environment, some flexibility of the target distribution is allowed. It is important to note that the coordinates of the spherical targets are not needed, and the only requirement is that they should remain static during the local survey.

The TLS range measurements are best described in a polar coordinate system centered at TLS, and the coordinates of a measured point in the mapping frame can be calculated as described by Eq. (3).

$$\begin{cases} x_p = x_c + s \cdot \cos \beta \sin \alpha \\ y_p = y_c + s \cdot \cos \beta \cos \alpha \\ z_p = z_c + s \cdot \sin \beta \end{cases} \quad (3)$$

where (x_p, y_p, z_p) and (x_c, y_c, z_c) are the vectors of coordinates of a measured point (here: spherical targets) and the laser scanner, respectively, in the mapping frame, s is the distance from the laser scanner to the target, α is the azimuth, and β denotes the vertical angle; s , α , β are measured by TLS.

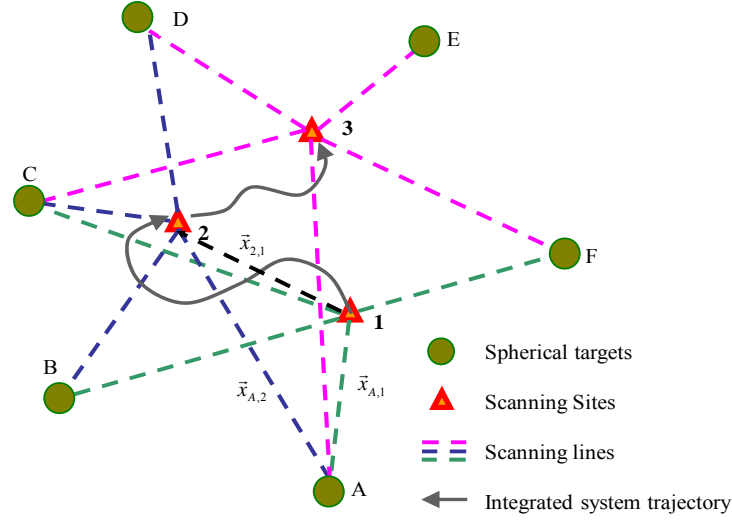


Figure 6. The spatial (3D) or partial resection (2D) concept using TLS ranges and spherical targets (Grejner-Brzezinska et al., 2008).

The coordinates of the centers of the spherical targets (points A-F in Figure 6), relative to the TLS coordinate system, can be calculated, as explained in the previous section. To simplify the computations, a local coordinate system is introduced, with the origin at site 1 (Figure 6). The spatial relationship between the two consecutive TLS locations, 1 and 2, with respect to target A, can be described by a rigid body transformation, including three offsets and three rotation angles (Eq. (4)).

$$\vec{x}_{A,1}^{b1} = \vec{x}_{2,1}^{b1} + R_{b2}^{b1} \vec{x}_{A,2}^{b2} \quad (4)$$

where $\vec{x}_{A,2}^{b2}$ is the translation vector from site 2 to point A in the local TLS coordinate system of site 2, $\vec{x}_{2,1}^{b1}$ is the translation vector from site 1 to site 2 in the local TLS coordinate system of site 1, $\vec{x}_{A,1}^{b1}$ is the coordinate vector from point 1 to site A in the local TLS coordinate system of site 1, and R_{b2}^{b1} is the rotation matrix from the local TLS coordinate system of site 2 to that of site 1. For multiple points, Eq. (4) can be expressed in a matrix form:

$$X_{P,1}^{b1} = X_{2,1}^{b1} + R_{b2}^{b1} X_{P,2}^{b2} \quad (5)$$

where P denotes all common targets observed at sites 1 and 2. In Eq. (5) there are six unknown parameters: the three translation parameters in $X_{2,1}^{b1}$, and the three Euler angles in R_{b2}^{b1} . To arrive at a more convenient expression, Eq. (5) is multiplied by the rotation matrix R_{b1}^n , from TLS coordinate system of site 1 to the navigation coordinate system (e, n, u); and then, the coordinate transformation, expressed in the navigation coordinate system, is given by:

$$R_{b1}^n X_{P,1}^{b1} = X_{2,1}^n + R_{b2}^n X_{P,2}^{b2} \quad (6)$$

Adding the coordinates of site 1 in the navigation frame to both sides of Eq. (6), considering that $X_2^n = X_1^n + X_{2,1}^n$, gives:

$$X_1^n + R_{b1}^n X_{P,1}^{b1} = X_2^n + R_{b2}^n X_{P,2}^{b2} \quad (7)$$

Eq. (7) can be linearized assuming small angular differences in the rotation matrix:

$$X_1^n + R_{b1}^n X_{p,1}^{b1} = X_2^{n0} - \delta X_2^n + (I - E) R_{b2}^{n0} X_{p,2}^{b2} \quad (8)$$

where I is the identity matrix, E is the skew-symmetric matrix of the attitude angle error, and δX_2^n is the coordinate error vector. Rearranging Eq. (8) provides the final positioning and attitude determination equation that is fed directly to the Kalman filter (Eq. 9). Note that it contains information that can be used to calibrate some of the IMU errors.

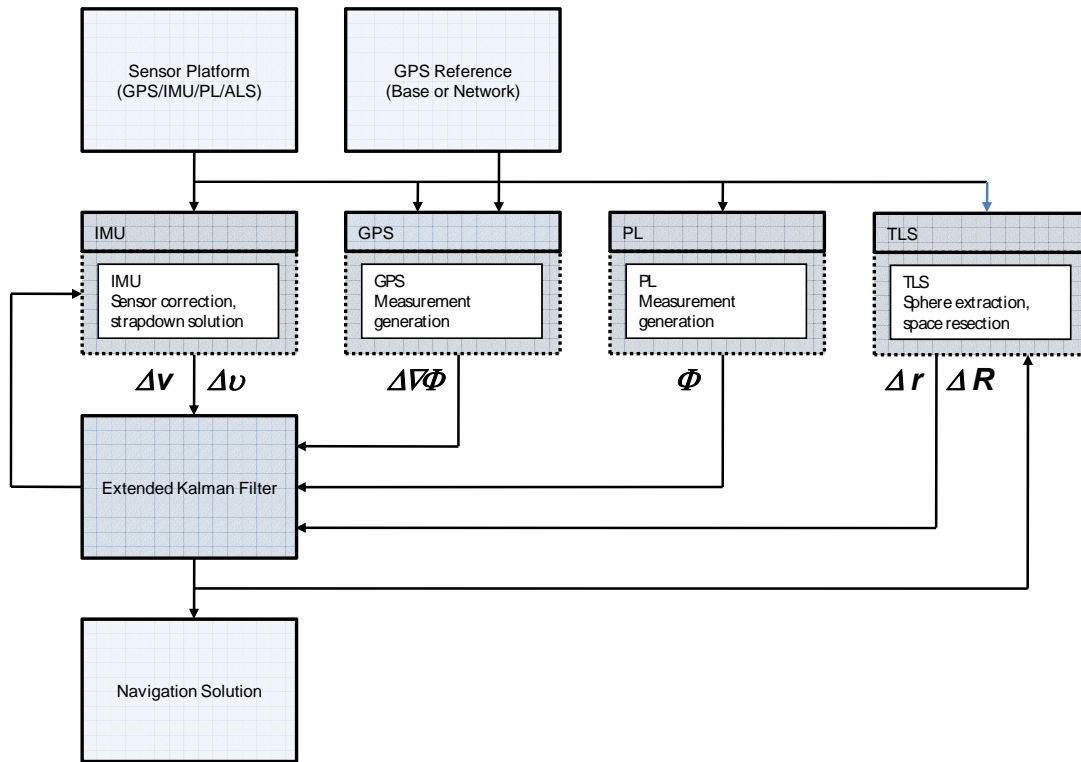
$$X_1^n + R_{b1}^n X_{p,1}^{b1} - X_2^{n0} - R_{b2}^{n0} X_{p,2}^{b2} = -\delta X_2^n + X_{p,2}^{n0} \mathcal{E} \quad (9)$$

where \mathcal{E} is the attitude angle error vector, and $X_{p,2}^{n0}$ is the skew-symmetric matrix of the coordinate vector. Note that the relative accuracy provided by Eq. (9) might be high, but the resulting absolute navigation accuracy depends on the accuracy of the position and attitude of site 1, which is assumed to be determined by the integrated DGPS/PL/INS.

4. SYSTEM IMPLEMENTATION

The system architecture, illustrated in Figure 7, represents an extension and major re-design of the original OSU GPS/IMU integrated system, AIMS™ (e.g., Grejner-Brzezinska and Toth, 1998; Grejner-Brzezinska, 1999). The novel *quadruple* integration of GPS (GNSS), PL and inertial technologies, augmented by TLS, replace the GPS/IMU integration module of AIMS™. The following are the primary characteristics of the AIMS-PRO™ system and software design:

- Handles various IMU classes, from navigation through tactical to consumer-grade sensors
- Loose and tight integration modes (tight mode illustrated in Figure 7)
- Implements feedback from the imaging module to implement terrain-referenced navigation in GPS-challenged environments
 - TLS with specialized targets for highest navigation accuracy
 - Airborne laser scanning (ALS)
 - Multiple image overlap-based relative orientation from optical imagery, DEM/GIS, etc.
- Multiple approaches to GPS solution (in loose integration mode):
 - Single baseline differential kinematic solution
 - Network-based differential kinematic solution
 - Precise point positioning technique (PPP)
- Post-processed and real-time capable
- Flexible design structure
- Extended error diagnostic capabilities



Note that RF spaceborne (GPS) and ground (PL) networks are not shown.

Figure 7. AIMS-PRO™ design architecture for the tight coupling mode, where Δv and $\Delta \omega$ are the rates of linear and angular velocities, respectively, Φ is the carrier phase range, $\Delta \nabla \Phi$ denotes the double-difference operator, and Δr and ΔR are linear and angular offsets between two TLS sites.

5 PERFORMANCE EVALUATION TEST

5.1 GPS/PL/IMU integration

Test data were collected at the Locata Inc., Numerella Test Facility, near Canberra, Australia, in March 2008. The sensor configuration, mounted on the top of a truck, included a Leica 1200 dual-frequency GPS receiver, H764G IMU and a Locata receiver, as shown in Figure 8 (note that additional sensors, IMU C-MIGITS2 and OmniStar receiver shown in the figure were not used in the tests discussed here). The detailed specifications of the sensors are listed in Table 3. The lever arm offsets of the GPS and Locata antennas were fixed and surveyed in the IMU body frame. The average separation between the rover and the base GPS was about 1.2 km, with the number of satellites observed being 5-9, and PDOP ranging from 1.9 to 4.8. There were ten LocataLites deployed in the test field and more than five of them were observed at every epoch of the test. Locata system was synchronized with the GPS time (Rizos et al., 2008). An example test trajectory is shown in Figure 9.

Since the primary interest here is the impact of the Locata signals on the overall navigation accuracy, the experiment discussed below focuses on the simulated GPS outages marked in red in Figure 9 and marked in Figures 10-13 as (in seconds within the week): 94099-94250 (151 s) and 94500-94601 (101 s).

The 3D navigation errors of the HG764G during two GPS outages were around 40 m and 13 m, respectively. These relatively large errors should be attributed to quite extensive maneuvering during the GPS outage that contributed to the increased errors in the yaw angle, resulting in substantial coordinate error in the transverse direction (the error along the trajectory is ~ 1m). In the navigation solution, where Locata signals compensated for the GPS outages, the accuracy was equivalent to the GPS/IMU solution. Figures 10-12 show the standard deviation of position, velocity and attitude, respectively, and Figure 13 illustrates the EKF position error state for the GPS/Locata/IMU solution.

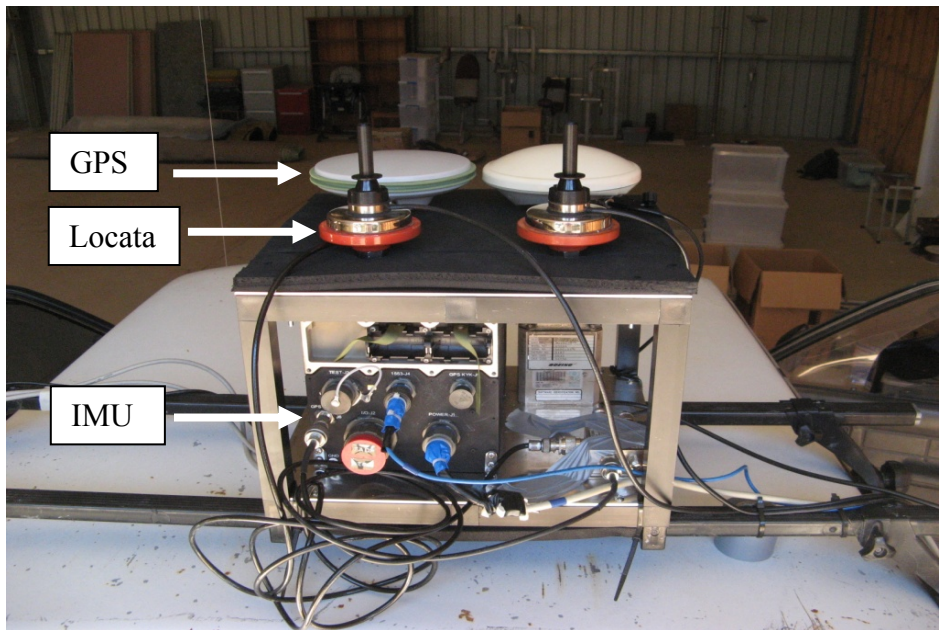


Figure 8. The sensor assembly used in the performance evaluation test.

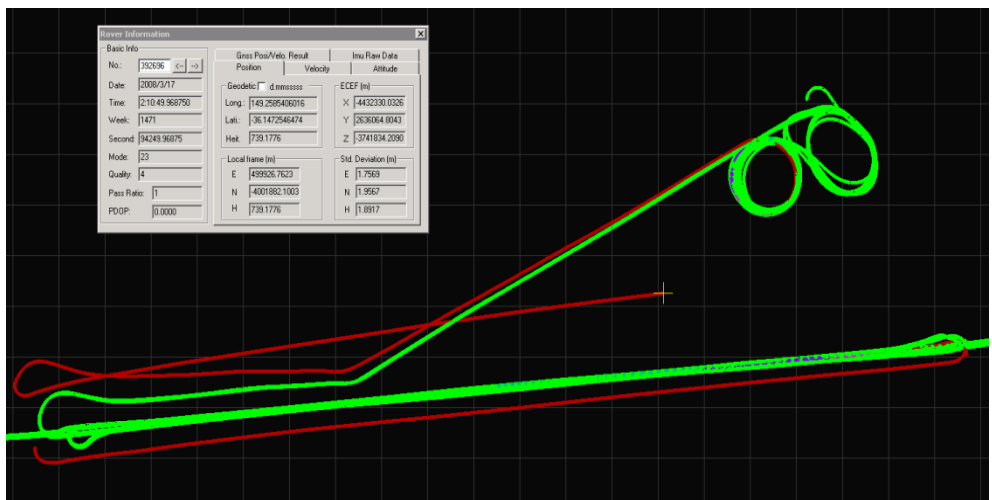


Figure 9. The test trajectory with the simulated GPS outages marked in red.

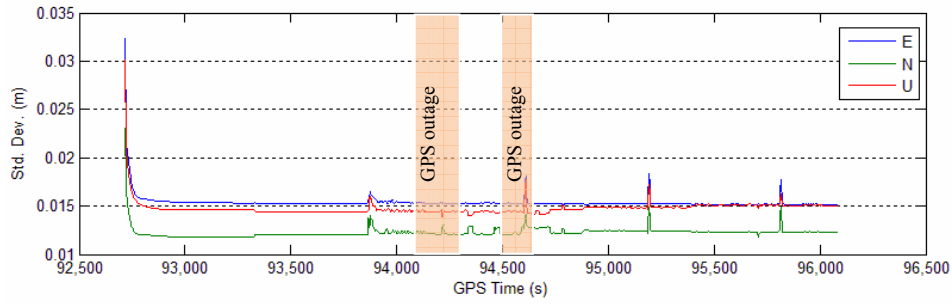


Figure 10. The standard deviation of the position coordinates in the GPS/INS/Locata solution.

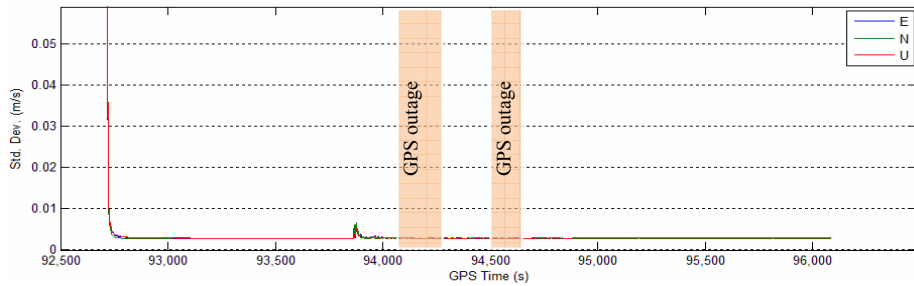


Figure 11. The standard deviation of the velocity components in the GPS/INS/Locata solution.

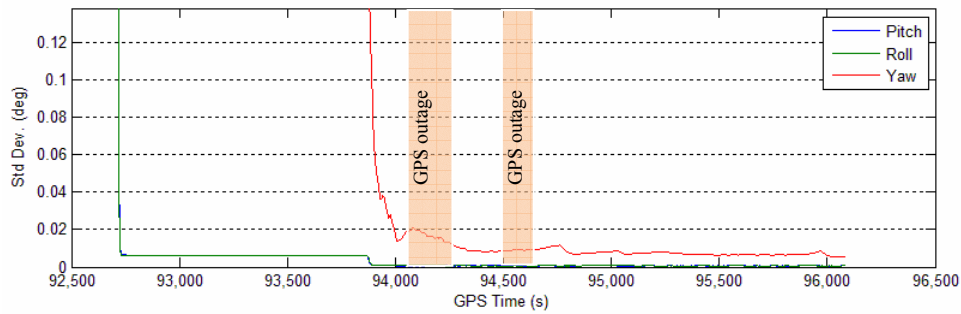


Figure 12. The standard deviation of the attitude angles in the GPS/INS/Locata solution.

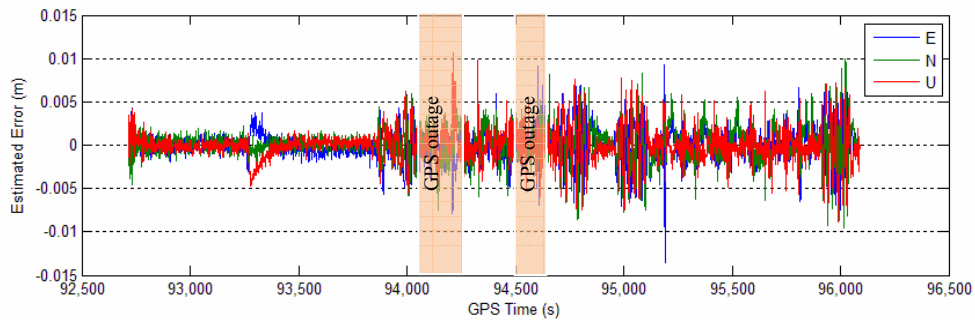


Figure 13. The EKF position error sub-state in the GPS/INS/Locata solution.

5.2 GPS/PL/IMU/TLS integration

During the GPS and Locata signal blockage, the system's accuracy is based on the INS stand-alone navigation. However, if the TLS is available, it can calibrate the IMU sensor errors, and consequently maintain the system's navigation accuracy in

the free-inertial navigation mode for the TPS update point. Simulated TLS data were used in the test to validate the efficiency of the TLS calibration. As illustrated in Figure 14, about 200 seconds of GPS and Locata data between points P0 and P1 were deleted to simulate the total loss of lock. During this time period, two TLS sites, A and B, were assumed, and the scanning data of six spherical targets (marked 1-6 in Figure 14) located in the vicinity of sites A and B were simulated with a noise level of 5 millimeters. The details of this simulated data are listed in Tables 4 and 5.

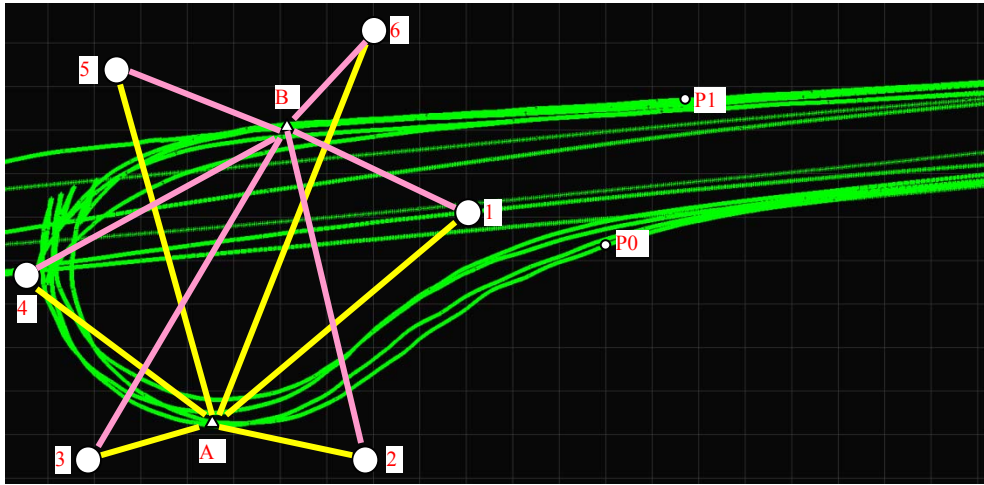


Figure 14. Test trajectory and the simulated TLS locations, A and B, and spherical target locations: 1-6.

The data were processed in three scenarios: (1) GPS/Locata/IMU integration (reference solution), (2) GPS/Locata/IMU solution followed by the free navigation mode based on H764G only, during the simulated GPS/Locata loss of lock, and (3) GPS/Locata/IMU solution followed by the IMU/TLS integration during the simulated GPS/Locata loss of lock. The navigation solutions for all three scenarios are listed in Tables 6 and 7.

By inspecting the results at point P1, listed in Table 6, it is clear that the TLS limits the IMU errors, reducing the 3D navigation error from 2.41 m (solution 2) to 0.12 m (solution 3) with respect to the reference trajectory (solution 1). Notice that the 12 cm absolute error results from the noise in TLS data and the fact that the system was navigating in a free-inertial mode for 6 seconds between points P0 and A and for 29 seconds between points B and P1. Similarly, Table 7 shows that the TLS-based calibration was able to reduce errors in the attitude angles, the yaw angle in particular.

The differences between the TLS-supported navigation solution (scenario 3) with respect to the reference trajectory (scenario 1) at points A and B are at the cm-level for the coordinates, and less than 0.0004° for the attitude angles, as listed in Tables 6 and 7. This clearly indicates that TLS can calibrate the IMU errors, while the free-inertial navigation solution (scenario 2) at points A and B is subject to errors ranging from 0.5 m to 1.8 m per coordinate component, and a heading error of up to 0.004° .

As can be observed in equation (9), the coefficient matrix for the coordinates is the identity matrix, which indicates that the coordinate calibration by TLS feedback is very stable, and the navigation accuracy is at the level comparable to the estimation accuracy of the spherical target center coordinates, which depends on the noise in the TLS range measurements, which increases with the distance to the target. Thus, the navigation solution calibration is more efficient for shorter TLS-target distances, and it does not depend on the TLS-target geometry. However, the coefficient matrix of the attitude angles is the skew-symmetric matrix containing coordinate offsets between the targets and the scanning sites, which indicates that the calibration performance for attitude angles is influenced not only by the distances between the TLS and the targets, but also by the distribution of the targets. Moreover, the error in target coordinate due to TLS range noise can translate into a significant angle error if the distances between the scanning site and the targets are too short. In the test presented here, the target coordinate error due to TLS range noise was set to 5 mm, and the average distance between the scanning sites and the targets was about 9 meters. The test result confirms the outcome due to the noise simulated by the error propagation in equation (9). The navigation error mitigation achieved by TLS comes together with the IMU error mitigation, as can be observed in Tables 6 and 7, by comparing scenarios 2 and 3 at points B and P1 after 165 s and 29 s GPS gaps, respectively. The free-inertial navigation following the TLS error reset is subject to coordinate errors about 100 times smaller than those of the free navigation mode without TLS calibration. The average IMU errors for the steady state part of trajectory are listed in Table 8.

5.3 Estimation of spherical target center coordinates and target matching based on field data set

Actual TLS data were collected on the West Campus parking lot of The Ohio State University in June 2008, to test the surface matching and the spherical target center coordinate determination algorithms. Ten spherical targets were placed along the service roads of the parking lot, as shown in Figure 15. A Trimble GX 3D laser scanner mounted on the top of a vehicle (Figure 15) scanned this area from different scanning locations; note that only two selected scans were considered in this discussion.



Figure 15. The spherical targets (left) and the scanning sensor (right).

In this test, the coordinates of the laser scanner were set to (0.0, 0.0, 0.0). The coordinates of the laser points range from 20 meters to 160 meters in the X direction, from -20 to -160 meters in the Y direction, and from -2 to 6 meters in the Z direction. The points on the spheres were matched using the algorithm described earlier, and the results of the center coordinate estimation are listed in Table 8. As listed in Table 8 (and Table 9 for scan 2), the accuracy of the estimated target centers is generally better than 1.5 millimeters, and the algorithm converged in three iterations, even when less than 70 points were available on the spherical surface. The point clouds of an example target are shown in Figure 16.

The second data set consists of 1879047 scanned points. The coordinates of the scanner were arbitrarily set to (9144.0, 9144.0, 302.0) and the coordinates of the laser points range from 9144 meters to 9325 meters in the X direction, from 9011 to 9144 meters in the Y direction, and from 300 to 308 meters in the Z direction. The results of the target center estimation are comparable to scan 1, and are listed in Table 9. The average difference in distances between any two given targets observed from two scanning sites (see Figure 17) is -2.2 mm with a corresponding standard deviation of 4.3 mm.

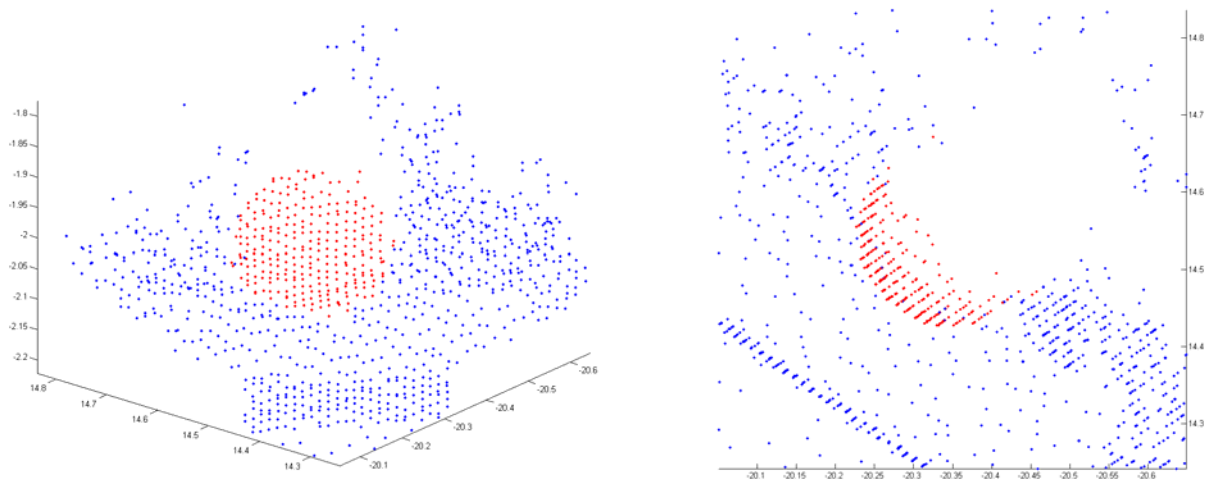


Figure 16. The extracted points of target 1 (red) and the neighboring points (blue). Left: side view, right: top view (m).

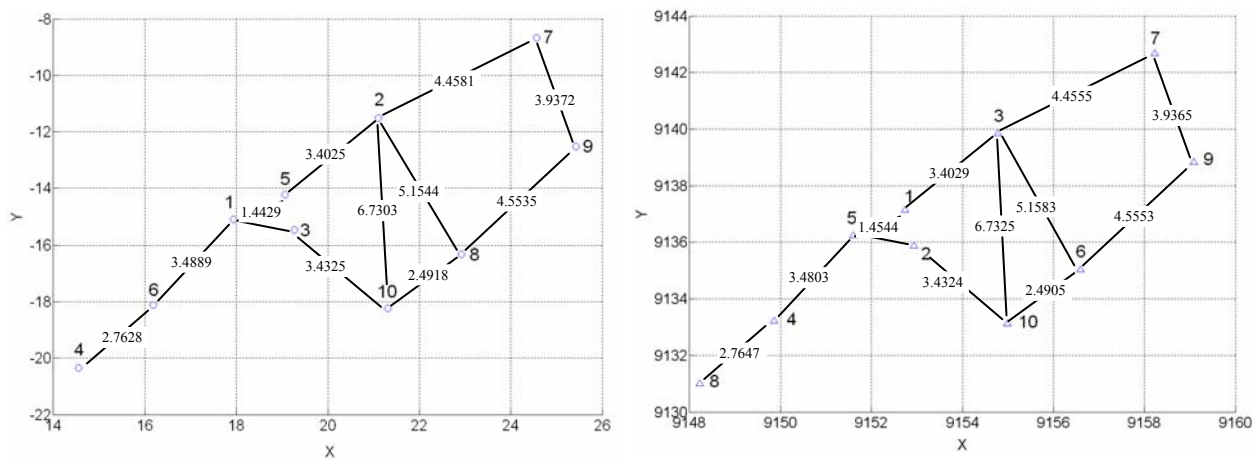


Figure 17. Estimated locations and corresponding connecting distances [m] of the spherical target centers of two TLS scans.

6. CONCLUSIONS

This paper describes the design and implementation of a *quadruple* integration system of GPS/INS/PL/TLS, used here as a navigation/geolocation tool. The system is currently under implementation, with GPS/INS/PL modules already implemented in the tightly-coupled mode under the EKF architecture, and the TLS module currently undergoing extensive simulation and real data testing. The results presented here demonstrated that both PL and TLS can maintain accurate INS calibration in the impeded environments where GPS is blocked. The integrated system provides cm-level absolute accuracy when GPS and/or PL signals are available, and is capable of maintaining sub-centimeter-level relative navigation, using spherical targets placed in the area of interest. The algorithms for spherical surface matching and center coordinate determination provide millimeter-level accuracy, as demonstrated using simulated and actual point cloud data collected in the field. The performance of the current system implementation can meet the accuracy requirement for EM sensor geolocation for MEC detection and remediation.

Acknowledgement: This research is supported by the 2007 SERDP grant. The authors wish to thank Nonie Politi and Yong Li from the University of New South Wales, and Joel Barnes and David Small of Locata Inc., for their support in field data collection.

REFERENCES

1. Abdullah, Q., (1997). Evaluation of GPS-Inertial navigation system for airborne photogrammetry, presented at 1997 ACSM/ASPRS Annual Convention and Exposition, 7-10 April, Seattle, WA.
2. Barnes, J., C. Rizos, J. Wang, D. Small, G. Voigt & N. Gambale (2003a). Locata: A new positioning technology for high precision indoor and outdoor positioning, 16th Int. Tech. Meeting of the Sat Div of the U.S. Inst. of Navigation, Portland, OR, 9-12 September, 1119-1128.
3. Barnes, J., C. Rizos, J. Wang, D. Small, G. Voigt & N. Gambale (2003b). High precision indoor and outdoor positioning using LocataNet, 2003 Int. Symp. on GPS/GNSS, Tokyo, Japan, 15-18 November, 9-18, CD ROM.
4. Barnes, J., C. Rizos, M. Kanli, A. Pahwa, D. Small, G. Voigt, N. Gambale & J. Lamance (2005). High accuracy positioning using Locata's next generation technology, 18th Int. Tech. Meeting of the Sat. Div. of the Institute of Navigation, Long Beach, CA, 13-16 Sept, 2049-2056.
5. Barnes, J., C. Rizos, M. Kanli & A. Pahwa (2006). A solution to tough GNSS land applications using terrestrial-based transceivers (LocataLites), Proceedings, Symposium on GPS/GNSS (IGNSS2006), Surfers Paradise, Australia, 17-21 July, CD-ROM.
6. Barnes, J., J. Lamance, B. Lilly, I. Rogers, M. Nix & A. Balls (2007). An integrated Locata & Leica Geosystems positioning system for open-cut mining applications, Proceedings, ION GNSS, September 25-28, Fort Worth, TX, CD ROM.
7. Dai, L., C. Rizos & J. Wang (2001). The role of pseudo-satellite signals in precise GPS-based positioning, *Journal of Geospatial Eng., HK Inst. of Engineering Surveyors*, 3(1), 33-44.
8. Elrod, B., K. Bartrop, J. Stafford & D. Brown (1996). Test results of local area augmentation with an in-band pseudolite, Proceedings, ION NTM, Santa Monica, CA, 22-24 January, 145-154.
9. El-Sheimy, N., & K.P. Schwarz (1999). Navigating urban areas by VISAT – A Mobile Mapping System integrating GPS/INS/Digital Cameras for GIS application, *Navigation*, 45(4), 275-286.
10. Grejner-Brzezinska, D.A., R. Da & C. Toth (1998). GPS error modeling and OTF ambiguity resolution for high-accuracy GPS/INS integrated system, *J. of Geodesy*, 72(11), 628-638.

-
11. Grejner-Brzezinska, D.A. (1999). Direct exterior orientation of airborne imagery with GPS/INS system: Performance analysis, *Navigation*, 46(4), 261-270.
 12. Grejner-Brzezinska, D.A. (2001a). Mobile Mapping Technology: Ten years later, Part I, *Surveying and Land Information Systems*, 61(2), 79-94.
 13. Grejner-Brzezinska, D.A. (2001b). Mobile Mapping Technology: Ten years later, Part II, *Surveying and Land Information Systems*, 61(3), 83-100.
 14. Grejner-Brzezinska, D.A., & Y. Yi (2003). Experimental GPS/INS/Pseudolite system for kinematic positioning, *Survey Review*, 37(288), 113-126.
 15. Grejner-Brzezinska, D.A., C. Toth & Y. Yi (2005). On improving navigation accuracy of GPS/INS systems, *Photogrammetric Engineering & Remote Sensing*, April 2005, 71(4), 377-389.
 16. Grejner-Brzezinska, D.A., C. Toth, H. Sun, X. Wang & C. Rizos (2008). GPS/INS/PL/TLS integration supporting navigation of geophysical sensors for unexploded ordnance detection and discrimination, Proceedings, 13th FIG International Symposium on Deformation Measurements and Analysis, 4th IAG Symposium on Geodesy for Geotechnical and Structural Engineering, May 12-15 2008, Lisbon, Portugal, paper 19, CD ROM.
 17. Gruen, A., & D. Akca (2005). Least squares 3D surface matching, Proceedings of ASPRS 2005 Annual Conference, Baltimore, MD, 7-11 March, CD ROM.
 18. Klein, D., Parkinson, B.W. (1986): The use of pseudo-satellites for improving GPS performance, Global Positioning System, Vol. III, Institute of Navigation, Washington, DC.
 19. LeMaster, E.A., M. Matsuoka & S.M. Rock (2003). Mars navigation system utilizes GPS, *IEEE Aerospace and Electronics Systems Magazine*, 18(4), April 2003, 3-8.
 20. LeMaster, E.A., & S.M. Rock (1999). Mars exploration using self-calibrating pseudolite arrays, Proceedings, ION GPS-1999, Nashville, TN, 14-17 September, 1549-1558.
 21. Montefusco, C., J. Ventura-Traveset, R. Lucas-Rodriguez, F. Toran, and M. Jofre (2005): Enhancing SBAS performance: the EGNOS pseudolite concept (http://www.egnos-pro.esa.int/Publications/EGNOS%20pseudolite%20ENC%202005_final.pdf, last accessed on April 3, 2008).
 22. Mostafa, M., J. Hutton & E. Lithopoulos (2000). Ground accuracy from directly georeferenced imagery, *GIM International*, 14(12), 38-41.
 23. SERDP, Strategic Environmental Research and Development Program (2005). SON NUMBER: MMSO-07-01, 10 November 2005.
 24. Shan, J. and C. Toth, Eds., (2008). Topographic Laser Ranging and Scanning: Principles and Processing, Published by Taylor and Francis.
 25. Progi, I.F., J. Maynard, W.R. Michalson & J. Wang (2006). The performance and simulation of a CCDMA pseudolite indoor geolocation system, Proceedings, ION-GNSS, Fort Worth, TX, 26-29 September, 3149-3162.
 26. Raquet, J., G. Lachapelle, W. Qiu, C. Pelletier, T. Nash, P. Fenton & T. Holden (1995). Development and testing of a mobile pseudolite concept for precise positioning, Proceedings, ION GPS, Palm Springs, CA, 12-15 September, 817-826.
 27. Rizos, C., D.A. Grejner-Brzezinska, C. Toth, A.G. Dempster, Y. Li, N. Politi, J. Barnes, & H. Sun (2008). A hybrid system for navigation in GPS-challenged environments: Case study, Proceedings, ION GNSS, Savannah, Georgia, 16-19 Sept, 1418-1428.
 28. Skaloud, J., (2002). Direct georeferencing in aerial photogrammetric mapping, *Photogrammetric Engineering & Remote Sensing*, March 2002, 207-210.
 29. Toth, C., & D.A. Grejner-Brzezinska (1998). Performance analysis of the Airborne Integrated Mapping System (AIMSTM), ISPRS Commission II Symposium on Data Integration: Systems and Techniques, *International Archives of Photogrammetry and Remote Sensing*, Vol. XXXII, Part 2, 320-326.
 30. Toth, C. (2002). Sensor integration in airborne mapping, *IEEE Transactions on Instrumentation and Measurement*, 51(6), 1367-1373.
 31. Veth, M., and J. Raquet (2006). Fusion of low-cost imaging and inertial sensors for navigation, Proceedings, ION GNSS, Fort Worth, TX, 26-29 September, CD ROM.
 32. Yi, Y., D.A. Grejner-Brzezinska & C. Toth (2005). Performance analysis of a low cost MEMS IMU and GPS integration, Proceedings, ION Annual Meeting, 26-29 June, 1026-1036.

System	Advantage	Disadvantage
GPS	Absolute position solution Accurate position/velocity	Line-of-sight system
PL	Absolute position solution Works well in confined environment (function of geometric configuration)	Line-of-sight system
INS	Self-contained system	Relative position solution Position drifts with time
TLS	Accurate position and attitude in a local reference frame	Relative position solution

Table 1. Rationale for sensor integration, based on their complementary characteristics.

Components	Characteristics	
Signal structure	Frequencies	Dual frequency 2.4 GHz (80 MHz bandwidth)
	PRN code	Proprietary (10 MHz chipping rate)
	License requirements	None required, FCC compliant
LocataLite (transceiver)	Hardware	FPGA & DDS technology with a modular design
	Output power	Maximum of 1 Watt
	Range	10km line-of-sight
	Antenna	Two TX antennas for spatial diversity
Locata (receiver)	Hardware	FPGA technology, modular design
	Measurement rate	25Hz
	Initial phase bias resolution	On-The-Fly

Table 2. Specification summary of the second generation of the LocataNet system (Barnes et al., 2005).

Specifications	IMU	BASE GPS	ROVER GPS	PL
Brand	H764G	Leica dual frequency	Leica dual frequency	Locata
Data rate	256Hz	1Hz	1Hz	1Hz
Gyro drift	0.0035deg/h, 0.0035deg/h ^{1/2} , sf=5ppm			
Accerolometer bias	25µg , 8.3µg (100Hz bw), sf=100ppm			

Table 3. The specifications of the sensors in the test; sf = scale factor; ppm = part per million; bw = bandwidth.

Point	Time (second within the week)	GPS gap (s)	Accumulated GPS gap duration (s)
P0	95324	0	0
A	95330	6	6
B	95495	165	171
P1	95524	29	200

Table 4. The simulated test points and the corresponding GPS gap duration along the test trajectory for TLS-based IMU calibration.

Site	Sphere	Distance (m)	Horizontal Angle (deg)	Vertical Angle (deg)	Right (m)	Front (m)	Height (m)	Right Noise (m)	Front Noise (m)	Height Noise (m)	Notes
A	1	8.205	134	-2	5.89859	-5.69620	-0.28635				Simulated
	2	5.720	194	-1	-1.38358	-5.54925	-0.09983				Simulated
	3	4.683	330	3	-2.33829	4.05004	0.24509				Simulated
	4	6.890	34	1	3.85225	5.71120	0.12025				Simulated

	5	14.217	57	-2	11.91612	7.73842	-0.49617				Simulated
	6	15.800	105	-2	15.25233	-4.08685	-0.55141				Simulated
B	1	6.717	52.80536	-1.87283	5.34956	4.05023	-0.21451	-0.002	-0.002	0.001	Calculated
	2	12.519	80.61644	-3.06223	12.33654	2.03917	-0.67776	0.003	0.001	0.002	Calculated
	3	13.148	124.76894	-2.60668	10.78324	-7.48005	-0.59696	-0.002	0.000	0.001	Calculated
	4	8.692	149.65537	-1.43583	4.39877	-7.49477	-0.21480	-0.001	0.003	0.001	Calculated
	5	8.353	208.20292	-1.17915	-3.94554	-7.36936	-0.16288	0.001	0.002	0.001	Calculated
	6	6.406	320.22152	2.65373	-4.08324	4.91982	0.28959	0.001	0.002	-0.002	Calculated

Table 5. TLS simulated data in the TLS scanning frame. Target coordinates at site A were simulated arbitrarily; target coordinates at site B were calculated based on the simulated target coordinates at site A and GPS/INS/Locata integrated navigation trajectory.

Site	Scenario	East (m)	North (m)	Height (m)	ΔE (m)	ΔN (m)	ΔH (m)
A	1	499629.2262	-4001953.4207	740.0301			
	2	499629.2470	-4001953.4151	740.0214	0.0208	0.0056	-0.0087
	3	499629.2470	-4001953.4151	740.0214	0.0208	0.0056	-0.0087
B	1	499630.5420	-4001943.4733	740.0877			
	2	499629.1573	-4001944.5292	740.5873	-1.3847	-1.0559	0.4996
	3	499630.5614	-4001943.4680	740.0790	0.0206	0.0053	-0.0087
P1	1	499643.6843	-4001942.5275	740.0575			
	2	499641.8912	-4001943.9805	740.7505	-1.7931	-1.4530	0.6930
	3	499643.7828	-4001942.5608	740.1109	0.0985	-0.0333	0.0534

Table 6. The coordinates in the three tested scenarios for GPS/IMU/PL/TLS integration.

Note: Scenario 1 denotes GPS/Locata/IMU integration; Scenario 2 denotes GPS/Locata/INS integration with simulated GPS/Locata outage; Scenario 3 denotes GPS/Locata/IMU/TLS integration with simulated GPS/Locata outage.

Site	Scenario	Pitch (deg)	Roll (deg)	Yaw (deg)	ΔP (deg)	ΔR (deg)	ΔY (deg)
A	1	-0.99049	-2.11935	84.71102			
	2	-0.99034	-2.11932	84.71130	0.00015	0.00003	0.00028
	3	-0.99034	-2.11932	84.71130	0.00015	0.00003	0.00028
B	1	-0.87873	-2.72638	279.67670			
	2	-0.87865	-2.72599	279.67341	0.00008	0.00039	-0.00329
	3	-0.87910	-2.72621	279.67677	-0.00037	0.00017	0.00007
P1	1	-0.25331	-3.69628	271.79831			
	2	-0.25278	-3.69590	271.79494	0.00053	0.00038	-0.00337
	3	-0.25319	-3.69619	271.79841	0.00012	0.00009	0.00010

Table 7. The attitude angles of the three tested scenarios for GPS/IMU/PL/TLS integration.

Output	X	Y	Z
Gyro drift (deg/h)	0.00044678	0.00120157	-0.00015568
Acce. Bias (mg)	0.00004722	-0.0003812	0.00038773
Gyro scale factor(ppm)	2.66	3.05	0.37
Acce. scale factor(ppm)	1.04	2.74	0.20

Table 8. The output of Kalman filter for IMU sensor errors.

Sphere	X (m)	Y (m)	Z (m)	Std. Dev. (mm)	Points	Iteration
1	17.932	-15.110	1.972	0.6	215	3
2	21.108	-11.501	1.835	0.7	197	3
3	19.064	-14.223	1.872	0.5	187	3
4	14.547	-20.351	2.011	0.7	187	3
5	19.262	-15.477	1.853	0.8	191	3
6	16.180	-18.125	1.918	0.8	172	3

7	25.420	-12.522	1.658	1.0	118	3
8	24.560	-8.682	1.759	0.9	106	3
9	22.918	-16.326	1.709	1.0	102	3
10	21.311	-18.230	1.792	1.5	67	3

Table 9. The coordinates of the estimated centers of the spherical targets in the first simulated TLS data set.

Sphere	X (m)	Y (m)	Z (m)	Std. Dev. (mm)	Points	Iteration
1	9152.737	9137.129	302.866	0.4	452	3
2	9152.935	9135.875	302.885	0.4	402	3
3	9154.775	9139.854	302.923	0.5	315	3
4	9149.854	9133.222	302.802	0.5	293	2
5	9151.595	9136.236	302.761	0.6	258	3
6	9156.593	9135.028	303.033	0.6	177	3
7	9158.223	9142.674	303.018	0.8	153	3
8	9148.219	9130.995	302.691	0.9	141	3
9	9159.092	9138.836	303.109	1.1	96	3
10	9154.989	9133.125	302.938	1.4	66	3

Table 10. The coordinates of the estimated centers of the spherical targets in the second TLS data set collected in the field